IEEE Access
Multidisciplinary | Rapid Review | Open Access Journal

Received February 11, 2020, accepted February 26, 2020, date of publication March 2, 2020, date of current version March 19, 2020.

Digital Object Identifier 10.1109/ACCESS.2020.2977696

Characteristics of Asymmetric Curls of a Halbach Hydroturbine Main Shaft Magnetofluid Sealing Device Under Random Rotational Speed Work Conditions

ZHENGGUI LI[1], JIE CHENG[1], DEYOU LI[2], XIAOHUI DENG[1], BING DONG[1], XIAOBING LIU[1], BIAO MA[1], AND XINRUI LI[1]

[1]Key Laboratory of Fluid and Power Machinery, Ministry of Education, Xihua University, Chengdu 610039, China
[2]School of Energy Science and Engineering, Harbin Institute of Technology, Harbin 150001, China

Corresponding authors: Zhenggui Li (lzhgui@mail.xhu.edu.cn) and Deyou Li (lideyou@hit.edu.cn)

This work was supported in part by the National Key Research and Development Program, China, under Grant 2018YFB0905200 and Grant SQ2018YFHZ010004, in part by the Chunhui Plan Project of the Ministry of Education (Study on Unsteady Cavitation Flow Characteristics in Flow Turbine Runners-2020), in part by the Sichuan Provincial Science and Technology Department Key Research and Development Plan Project under Grant 20GJHZ0125 and Grant 20SYSX0236, in part by the Open Research Subject of Key Laboratory (Fluid Machinery and Engineering Research Base) of Sichuan Province, China, under Grant szjj2019-001, and in part by the Open Fund of Key Laboratory of Fluid and Power Machinery, Xihua University, Ministry of Education, Sichuan, China, under Grant szjj2019-023.

ABSTRACT The operational rotational speeds of hydroturbines change arbitrarily within a small range, and the friction power consumption caused by the asymmetric curl represents a technical difficulty in magnetofluid sealing. In this study, the pressure-withstanding value and equations for the asymmetric curl of a magnetofluid sealing device under different rotational speeds were deduced. By considering the magnetofluid sealing device characteristics with Halbach magnetic arrays, temperature fields under a static field and low rotational speed were calculated for determining the Halbach magnetofluid sealing device with the best sealing performance. Comparisons and analyses were performed with the friction power consumption and sealing pressure-withstanding value of the selected structure under high (3000 r/min), medium (1500 r/min), and low (300 r/min) rotational speeds and alternating work conditions of ± 3, ± 6, and ± 9. The results indicated that changes in magnetic moment caused by changes in the external magnetic field are the primary cause of friction power consumption. Heat generation occurs concurrently with the friction power consumption. Consequently, the pressure-withstanding value of the magnetofluid sealing is reduced; the friction power consumption of the magnetofluid is directly proportional to the magnetic field strength, rotational speed, and alternating amplitude. Unstable states and asymmetry of the external magnetic field lead to nonlinear increments in the friction power consumption of the magnetofluid. A stable and symmetrical magnetic effect, with a smaller rotational speed and alternating amplitude leads to lower friction power consumption, resulting in a more ideal sealing effect.

INDEX TERMS Hydroturbine, magnetofluid sealing, Halbach magnetic array, friction power consumption, asymmetric curl.

I. INTRODUCTION

With the rapid development of the world economy, the population of the world has increased sharply. To adapt to the theme of the times, different countries around the globe are expending more effort to develop renewable energy. According to the Global Energy Report of 2018, the amount of global hydroelectric generation has reached 4185 TWh, and the total installed hydropower gross capacity is 1267 GW. Hydropower, accounting for 16.6%, has been ranked the top among all renewable energy types [1], [2].

For hydroelectric power generation, the main shaft of a hydroturbine is the key concern, as it directly impacts the quality of the electrical energy generated. However,

The associate editor coordinating the review of this manuscript and approving it for publication was Zhonglai Wang.

the bottleneck preventing the hydroturbine from achieving stable operation is the sealing technique used for the main shaft. Accidents and environmental pollution caused by main-shaft sealing failures have always been serious issues. For example, in the Tai'an Pumped Storage Hydropower Station in Tai'an City, Shandong Province, when the #2 unit starts to operate, the main shaft experiences serious leakage of water, and the head cover water level triggers a warning, which adversely impacts the operation of the unit [3]. Another example is the Wanmipo Hydropower Station. Since the initial stage, when the station started to operate, the main shaft has suffered seriously wear. The upward water flow at the lower part of the rotating wheel primarily passes the clearance of sealing and anti-wear rings and flows to the side of the main shaft. Consequently, the main shaft leaks large amounts of water [4]. The Laodukou Hydropower Station on the State Grid contains two 45 MW units, which were respectively put into production for power generation in July and September of 2008. However, since operations began, owing to a main shaft sealing problem, the equipment has been unable to jack up normally, and there has been substantial leakage of water at the head covers of the hydroturbines. Notably, the self-draining system cannot lower the water level of the head cover of the hydroturbine. To prevent the plant from being drowned by water, for each unit, two immersible pumps have been added for drainage. However, as indicated by the operation records during the flood season, this flaw has severely restricted the generating capacity of the stations. Additionally, a considerable fraction of the generated power has been wasted, and this issue threatens the operational safety of the units [5]. In the Guiguan Dahua Hydropower Station, Guangxi Province, there have been incidents caused by main shaft leakages of the hydroturbine, resulting in serious hydropower accidents [6]. Problems also have occurred at the Karun III Hydropower Station, one of four hydropower stations under the contract signed by Harbin Electric Machinery Company Limited and Iran. For the main-shaft sealing of the hydroturbine at the Karun III Hydropower Station, static-pressure self-regulating axial and end-face sealing have been applied. However, the clearance between the anti-wear ring and the sealing ring was set at an excessively large value large during installation; thus, water leakages from the unit during operation have been considerably larger than predicted values. The serious water leakages at the main shaft have adversely affected the normal operation of the unit [7].

For the main shaft of current hydroturbines, common sealing methods include radial direction spiral packing sealing, radial direction spiral labyrinth sealing, axial direction mechanical carbon sealing, axial direction carbon crystal (nylon) water pressure sealing, plate sealing, L-type sealing, and double-plate sealing. However, these traditional sealing methods cannot guarantee reliability, stability, and ''zero leaks.'' Furthermore, there are some disadvantages of these sealing structures that should be noted. For example, for radial direction spiral packing sealing, dewatering spun-yam is used as sealing material and is arranged along the inverse spiral direction of the water leak. Such a sealing method has poses relatively high requirements on the sealing materials, and its anti-wear performance has to be relatively strong. However, this sealing method has a relatively poor compensatory nature and the packing will cause wear on the shaft neck. For radial direction spiral labyrinth sealing, the anti-spiral choke flow principle is used for sealing, but the leak amounts are large and this method cannot be used for hydropower stations with large sediment concentrations. For radial direction spring balance carbon crystal sealing, the joint effect of water pressure and spring force achieves the sealing, but there is often unevenness in the spring force and this method can have a poor sealing performance. For radial mechanical carbon sealing, carbon blocks are used as sealing materials. The anti-wear performance is relatively good, and the friction force is small; however, the structure of this sealing method is complicated, and the technique is difficult. When the accuracy grade of the springs and manufacturing is not sufficient, the surrounding forces of the carbon blocks may not be evenly distributed. Therefore, the sealing is not that stable and cannot last for long periods of time [8]–[10]. Overall, there are many sealing methods for the main shaft of a hydroturbine, but there are obvious disadvantages to each. Thus, better sealing structures need to be developed to satisfy the sealing requirements of the main shaft of hydroturbines.

Currently, magnetofluid sealing, as a new sealing method with ''zero leaks,'' has become a hot topic in the sealing industry. Related studies can be dated back to the 1960s. American scholar Rosensweig [11] studied the sealing issue of the movable part on American space suits in a vacuum environment and applied this method in real practice. Since then, scholars worldwide have carried out numerous research on magnetofluid sealing. For instance, in 1980, Berkowitz *et al*. [12] studied the positive correlation between the bonding degree of magnetic-particles and surfactants and the magnetization intensity of magnetofluid by using methods that included chemical analyses, electron microscopy, X-ray diffraction, magnetic measurements, and Masbauer spectroscopy. In 1984, Kamiyama [13] studied liquid and air magnetofluid sealing and the results showed that for liquid magnetofluid sealing, the solvability between the magnetofluid and sealed liquid and the interface stability will directly influence the liquid magnetofluid sealing performance. In 1994, Bacri *et al*. [14] the behaviors of magnetofluid microdroplets in rotating magnetofluid fields; the results showed that under a magnetic field, the difference in the stability of the top end and tail end of a magnetofluid in a rotating magnetic field is significant, and furthermore, the magnetofluid rotation frequency is far lower than that of the magnetic field rotation frequency. In 2003, Kim and Kim [15] carried out an application study of a magnetofluid, and comparisons and analyses were made of the sealing pressure of the structure of a magnetofluid consisting of iron cobalt magnetic particles and normal magnetic particles; the results showed that the sealing

pressure of iron cobalt magnetofluid is 25 times than that of traditional magnetofluid, that is to say, the sealing performance is great. In recent years, more explorations of magnetofluid sealing have been conducted. For example, Hayat *et al*. [16], [17] combined the Soret and Dufour effect to study a magnetofluid, and their findings showed that under different physical parameters, the Casson number β and Hartman number Ha increase while the speed slows down. Hu *et al*. [18] studied the stability and mobility of a magnetofluid and put forward some suggestions on enhancing the stability of magnetofluids. Chi [19] published a book titled ''Fundamental and Application of Physics for Ferromagnetic Fluid,'' which systematically sorts through the hydrodynamic equations, thermodynamic equations, and optical equations of magnetofluids, thus providing a theoretical basis for researchers of magnetofluids. In regard to magnetofluid sealing, Li [20] published a book titled ''Theories and Applications of Magnetic Liquid Seal,'' which systematically introduces the reader to the preparation and related features of magnetofluids as well as some rules for magnetofluid sealing, thus providing a sound theoretical basis for magnetofluid sealing.

Based on the theories of magnetofluid sealing, the specific sealing method can be described as follows: fill the magnetofluid into the sealing clearances and set up special magnetic fields at the two sides of the sealing clearances. The magnetofluid is ''locked'' in the clearances to finally seal the device [21], [22]. The pressure-withstanding value of magnetofluid sealing is directly proportional to the intensity difference in magnetic induction of sealing clearances and the magnetofluid saturated magnetic strength, and the external magnetic field strength will change the nature of the magnetofluid and affect the intensity difference during magnetic induction of sealing clearances. Therefore, to optimize the magnetic field structure, one can, to a large extent, improve the sealing pressure-withstanding value of the magnetofluid. The Halbach magnetic array, as a new unilateral strengthened structure of a magnetic field, was discovered by American scholar Mallianson in the 1970s. Later, in 1979, when the American scholar Lund and Halbach [23] and Halbach [24] was performing experiments on electron acceleration, he optimized the permanent magnet configuration. A Halbach magnetic array refers to magnetic blocks configured according to certain rules, and the interaction between these blocks can form a special unilateral strengthening of magnetic energy. Compared with other ordinary permanent magnet configurations, Halbach has a considerably higher utilization rate of magnetic energy.

Therefore, in this study, four typical Halbach magnetic arrays were applied in the magnetofluid sealing device of a hydroturbine. The pressure-withstanding value and asymmetric curl of the magnetofluid sealing device with different Halbach magnetic arrays under different rotational speeds were analyzed to provide a theoretical basis for the application of magnetic arrays in magnetofluid sealing devices.

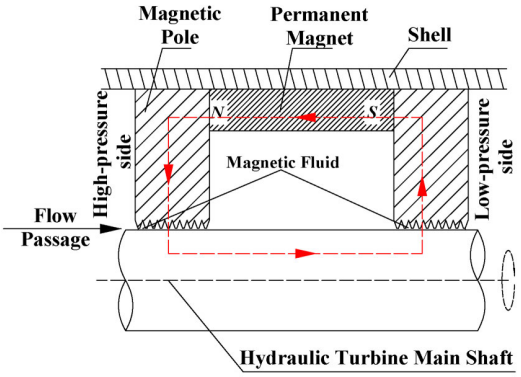

FIGURE 1. Schematic diagram of the magnetic fluid seal.

First, theoretical deductions were made on the equations for the pressure-withstanding value of a magnetofluid and the asymmetric curl. Then, ANSYS software was leveraged to respectively calculate the magnetic field and temperature field of each structure. Next, experiments were performed for each model to obtain the actual sealing pressure and friction power consumption. Lastly, the experimental results were referenced to analyze the relationship between the magnetic field and the friction power consumption to determine the optimal hydroturbine main shaft magnetofluid sealing method.

II. THEORETICAL EQUATIONS

A. MAGNETOFLUID SEALING EQUATION

Fig. 1 shows a schematic diagram of the magnetofluid sealing of a hydroturbine main shaft. There are five main components, namely, a main shaft, magnetic poles, magnetofluids, permanent magnets, and shells. The main shaft and magnetic poles provide the magnetic paths, which constrain the magnetic field; the magnetofluids serve as the sealing material and function as a sealing medium. The permanent blocks are the magnetic source of the entire device and provide the magnetic force; the shell protects the units inside. The magnetofluid sealing works as follows: the magnetic energy of permanent magnets starts from the N pole and follows the paths guided by the poles and the main shaft; finally, the energy flows to the S pole, before forming a magnetic loop. The magnetofluids, which are located between the magnetic poles and main shaft, are affected by the magnetic force; these are ''locked'' in the sealing clearances, and an ''O''-shaped sealed loop is formed to prevent the medium from being leaked from the high-pressure end to the low-pressure end, ultimately achieving the purpose of sealing.

According to the schematic diagram of the magnetofluid sealing, a simplified calculation diagram of the cylinder was mapped as shown in Fig. 2 (A is a point at the interface between the high-pressure side magnetofluid liquid and the sealed fluid; B is a point at the interface between the low-pressure side magnetofluid and air).

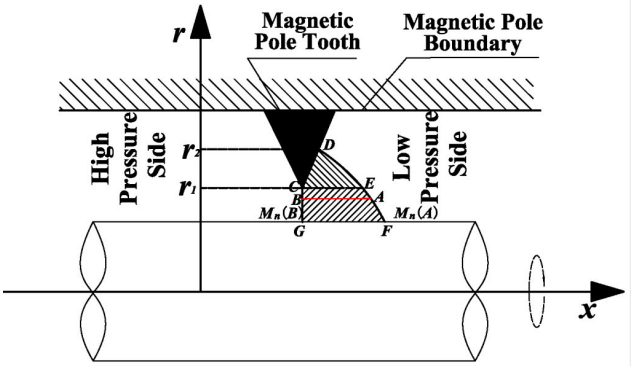

FIGURE 2. Cylinder standard calculation diagram.

According to earlier work [25], [26], the Bernoulli equation for the magnetofluid is:

$$p_0 + \frac{1}{2}\rho v^2 - \mu_0 \int_0^H MdH = C \tag{1}$$

where ρ is the density of the magnetofluid; v is the velocity of the magnetofluid micelles; p_0 is the magnetofluid pressure; M is the magnetization intensity of the magnetofluid; H is the strength of the magnetic field; C is a constant; and μ_0 is the vacuum permeability.

In joint consideration to (1) and Fig. 2, the Bernoulli equations at points A and B in Fig. 2 are:

$$p_0(A) + \frac{1}{2}\rho v_A^2 - \mu_0 \int_0^{H(A)} MdH = C \tag{2}$$

$$p_0(B) + \frac{1}{2}\rho v_B^2 - \mu_0 \int_0^{H(B)} MdH = C \tag{3}$$

In (2) and (3), $p_0(A)$, $_{p_0}(B)$ are the magnetofluid pressure and $H(A)$, $H(B)$ are the strength of the magnetic field at points A and B, respectively; v_A is the velocity of the magnetofluid micelles at point A; and v_B is the velocity of the magnetofluid micelles at point B.

At the interface, the pressure of the sealed liquid is represented by $p(A)$ and $p(B)$; therefore

$$p_0(A) + \frac{1}{2\mu_0} M_n^2(A) = p(A) \tag{4}$$

$$p_0(B) + \frac{1}{2\mu_0} M_n^2(B) = p(B) \tag{5}$$

In this equation, $Mn(A)$ and $M(B)$ are the components of the magnetization intensity of the magnetofluidat points A and B, respectively, perpendicular to the interface.

In overall consideration to the above equatios, the pressure difference betweenpoints A and B can be expressed as:

$$\begin{aligned} p(B) - p(A) = &-\frac{1}{2}\rho v_B^2 + \frac{1}{2}\rho v_A^2 \\ &+ \frac{1}{2\mu_0}(M_n^2(B) - M_n^2(A)) \\ &+ \mu_0 \int_{H(A)}^{H(B)} MdH \end{aligned} \tag{6}$$

Equation (7) can be simplified as follows:

$$\begin{aligned} p(B) - p(A) = &\frac{1}{\mu_0}\overline{M}(B_{\max} - B_{\min}) \\ &- \int_A^B \frac{1}{r}\rho v^2 dr \\ &+ \frac{1}{2\mu_0}\left(M_n^2(B) - M_n^2(A)\right) \end{aligned} \tag{7}$$

where M is the average magnetization intensity of the magnetofluid; B_{max} is the maximum magnetic induction intensity (high-voltage side-B), which is obtained at the point with the minimum clearance; and B_{min} is the minimum magnetic induction intensity (low-voltage side-A), which is obtained at the point with the maximum clearance.

According to the analysis of (7), the first item on the right side of the equal sign of the equation is the magnetic field force, the second item is the centrifugal force, and the third item is the internal magnetic field force of the magnetofluid liquid. In terms of the magnetofluid studied here, the interior of the small-clearance magnetofluid sealing device is uniform after the magnetization of the magnetofluid is stabilized, and the radial dimensions of points A and B are to the center of rotation of the main shaft, so the values of the vertical component of magnetization intensity are equal. On the basis of this reasoning, the simplified equation for the pressure resistance of the magnetofluid resulting from simplifying (7) is:

$$\begin{aligned} p(B) - p(A) = &\frac{1}{\mu_0}\overline{M}(B_{\max} - B_{\min}) \\ &- \int_A^B \frac{1}{r}\rho v^2 dr + \end{aligned} \tag{8}$$

According to the simplified equation, the pressure resistance of magnetofluid sealing is positively correlated to the difference in the magnetic induction intensity at the clearance and the product of magnetization intensity. Therefore, the difference in the magnetic induction intensity at the clearance of the magnetofluid sealing and magnetization intensity can be improved to reduce the rotational speed of the main shaft and enhance the pressure resistance of magnetofluid sealing, so as to maximize the sealing effect.

B. MAGNETOFLUIDIC FRICTION POWER CONSUMPTION EQUATION

In Fig. 3, which shows a schematic diagram of the shear flow of magnetofluid, (a) represents the rotational motion of the magnetofluid without magnetic action and (b) represents the rotational motion of the magnetofluid with magnetic action. According to the force analysis of the magnetofluid, the magnetofluid is driven by the main shaft to move circularly along the axis of the main shaft when the magnetic force working on the magnetofluid is zero. The magnetofluid will rotate eccentrically under the effect of the centrifugal force and magnetic force caused by the rotation of the main shaft when the magnetic force working on the magnetofluid is not zero, resulting in asymmetric rotation $\Omega \neq \frac{1}{2}(rot\ \mathbf{v})$ and frictional torque;

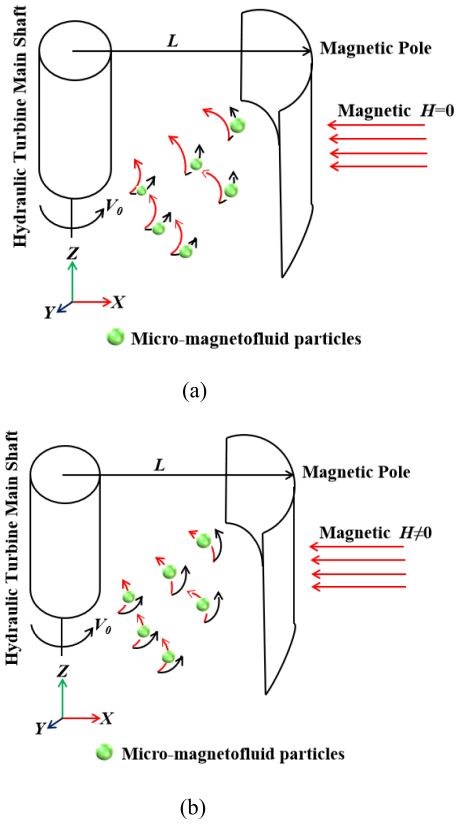

FIGURE 3. Schematic diagram of magnetic fluid shear flow: (a) H=0, (b) H≠0.

this will lead to frictional power consumption, increases in the temperature of the magnetofluid, significant reductions in the withstand voltage of the sealing, and decreases in the sealing effect [27]–[29].

According to the schematic diagram of the shear flow of magnetofluid without magnetic force in Fig. 3(b), the equation for the flow field of the magnetofluid under these conditions is:

$$\boldsymbol{v}\,(r) = v_0 \frac{z}{L}\left(\mathbf{e_x} + \mathbf{e_y}\right) \tag{9}$$

where v_0 is the rotation speed of the main shaft; z is the Z-axis coordinate; L is the distance from the main shaft axis to the magnetic pole boundary; e_x is the basis vector in the X direction; and e_y is the basis vector in the Y direction.

For magnetofluids subjected to an external magnetic force, the rotation equation is:

$$\boldsymbol{\Omega}_0\,(\mathbf{r}) = \frac{1}{2} rot\,\mathbf{v} = \frac{v_0}{2L}\mathbf{e_z} \tag{10}$$

where $\boldsymbol{e_z}$ is the basis vector in the Z direction.

When the magnetofluid is subjected to the magnetic field force as shown in Fig. 3(b), there is a deflection displacement M in both the Z and Y direction. This is expressed in the Shlionmis equation as

$$\text{div}\ \mathbf{v} = 0 \tag{11}$$

$$\rho\frac{d\mathbf{v}}{dt} = -\nabla p + Z\nabla\mathbf{v} + \frac{1}{2}Z_r rot\left(\boldsymbol{\Omega} - \frac{1}{2}rot\mathbf{v}\right) + \mu_0(\mathbf{M}\nabla)H \tag{12}$$

$$\frac{d\mathbf{M}}{dt} = -\frac{1}{f}\left(\mathbf{M} - \frac{M}{H}\mathbf{e_H}\right) + \boldsymbol{\Omega}\times\mathbf{M} \tag{13}$$

$$\theta\frac{d\boldsymbol{\Omega}}{dt} = -Z_r\left(\boldsymbol{\Omega} - \frac{1}{2}rot\mathbf{v}\right) + \mu_0\boldsymbol{\Omega}\times\mathbf{M} \tag{14}$$

where Z is the shear viscosity coefficient of the magnetofluid; Z_r is the rotational viscosity of the magnetofluid; f is the relaxation time of the magnetization intensity; θ is the average moment of inertia; and $\boldsymbol{e_H}$ is the basis vector in the magnetic field direction.

According to the static Maxwell equation of the magnetic field:

$$rot\mathbf{H} = 0\ div\ \mathbf{B} = 0 \tag{15}$$

Equation (15) can be placed into (11) to (14) when $\Omega_f \ll 1$, so:

$$\mathbf{M} = \Omega_f M\,(H)\left(-\mathbf{e_y} + \mathbf{e_z}\right) \tag{16}$$

$$\boldsymbol{\Omega} = \frac{1}{2}rot\mathbf{v} + \boldsymbol{\omega} \tag{17}$$

$$\boldsymbol{\omega} = \frac{fM\,(H)\,\mu_0 H}{\mu_r + fM\,(H)\,\mu_0 H}\Omega_0\mathbf{e_y} \tag{18}$$

where ω is the angular velocity under the action of the magnetic field force; and μ_r is the relative permeability of the magnetofluid.

Under the action of the external magnetic field, the friction torque of the magnetofluid is:

$$\int dV\,\mu_0\mathbf{M}\times\mathbf{H} = \int dVZ_r\boldsymbol{\omega} \tag{19}$$

where V is the total volume of the magnetofluid.

Additional friction torque ΔT will emerge when the magnetofluid is under an external magnetic force, thus resulting in the generation of heat. For convenience of calculations, function K(H) is adopted here; therefore

$$K\,(H) = Ve\,(H)\,K_0\Delta T \tag{20}$$

$$e(H) = \mu_0 H_0 M(H) \tag{21}$$

where H_0 is the magnetic field intensity in the magnetofluid; $M(H)$ is the magnetization intensity of the magnetofluid; and K_0 is Boltzmann's constant.

According to the magnetofluid magnetization equation [30]–[32], the magnetization intensity M(H) of the magnetofluid is:

$$M\,(H) = M_S\left(\coth\frac{\mu_0 H M_p V_{p1}}{K_0 T} - \frac{K_0 T}{\mu_0 H M_p V_{p1}}\right) \tag{22}$$

where M_p is the magnetization intensity of the solid phase of the magnetofluid; M_s is the saturation flux density of the magnetofluid; V_{p1} is the volume of each solid particle; and T is the absolute temperature of the magnetofluid.

According to the Maxwell equation for the magnetofluid [33], K(H) is:

$$K(H) = \frac{1}{f} + \frac{1}{Z_r} e(H) \tag{23}$$

According to (20) to (23), the additional friction torque is:

$$\Delta T = \frac{\frac{1}{f} + \frac{1}{Z_r}\mu_0 H_0 M(H)}{V H_0 M(H) K_0} \tag{24}$$

Then, the friction power consumption P is:

$$P = \boldsymbol{\omega} \times \boldsymbol{\Delta T} \tag{25}$$

The frictional power consumption of the magnetofluid in the external magnetic field can be calculated by the above equation.

III. NUMERICAL CALCULATION AND ANALYSIS

According to the magnetofluid sealing and friction power consumption equations described in the previous section, the external magnetic field strength and rotation speed are directly related to the sealing withstand voltage and friction power consumption. According to (9) for the magnetofluid sealing pressure resistance, the difference in the magnetic induction intensity at the clearance of the magnetofluid sealing is inversely proportional to the rotational speed of the main shaft and in direct proportion to the sealing pressure resistance; moreover, for the friction power consumption in (24) and (25), the frictional power consumption value has a nonlinear relationship with the external magnetic field intensity and speed. Therefore, simulation calculations are performed on four Halbach magnetic arrays with ANSYS finite element analysis software in this section to compare and analyze the magnetic field and temperature field distributions so as to identify a Halbach magnetic array structure with a high sealing pressure resistance value and low friction power consumption.

A. SIMULATION MODEL AND BOUNDARY CONDITIONS

1) INTRODUCTION TO THE SIMULATION MODEL

The overall schematic diagram of this simulation model, a tubular turbine set, is shown in Fig. 4. It mainly consists of a runner, magnetofluid sealing device, main shaft, bulb housing, lamp cap, and rotor. During running of the set, water flows along the direction of the runner and drives the runner on the lamp cap to rotate, which turns the water energy into mechanical energy of rotation. The lamp cap is a rotating part, and the bulb housing is a stationary part. Water in the runner will flow into the turbine along the clearance between the lamp cap and the bulb, in which there is electrical equipment such as a generator, which requires secure sealing to prevent water from flowing inside. Therefore, a magnetofluid sealing device is set on the main shaft of the turbine to prevent water in the runner from entering the generator.

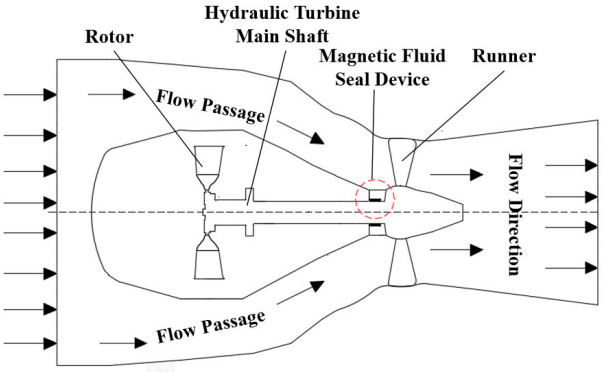

FIGURE 4. Overall view of the turbine.

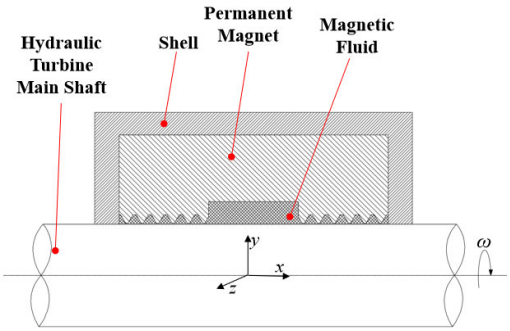

FIGURE 5. Magnetic fluid seal device diagram.

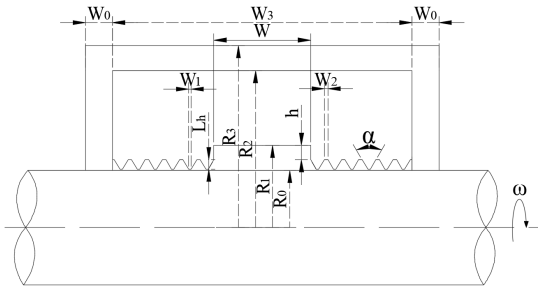

FIGURE 6. Dimensional schematic diagram of the magnetic fluid sealing device.

2) INTRODUCTION TO THE SEALING DEVICE

As shown in Fig. 5, the sealing device used for this simulation consists of the main shaft, housing, permanent magnet, and magnetofluid. The magnetic field generated by the permanent magnet passes through the sealing clearance and "locks" the magnetofluid inside the sealing clearance, so as to complete the sealing with an "O"-shaped sealing ring.

A schematic diagram of the size of the magnetofluid sealing device is shown in Fig. 6, and the specific size is given in Table 1.

3) BOUNDARY CONDITIONS

This simulation model is a tubular turbine set with a rotation speed of 300 r/min, rated head of 20 m, runner diameter of

TABLE 1. Turbine spindle magnetic fluid seal structure parameter table (unit: mm).

The diameter of the hydraulic turbine/R_0	Inside diameter of gap/R_1	Permanent magnet outer diameter/R_2	Shell outer diameter/R_3	Gap middle width/W	Shell thickness/ W_0	Magnetic slot width/W_1	Polar tooth width/W_2	Total seal length/W_3	Polar tooth angle α/°	Height of middle seal gap/h	Tooth height/L_h
40	55.4	80	90	10	5	0.5	0.5	60	60	5	2.5

TABLE 2. Thermodynamic parameters of magnetic fluid.

Material	Density ρ(kg/m^3)	Specific Heat Capacity c(J/kg·K)	Thermal Conductivity λ(W/m·K)	Thermal Expansion Coefficient $\beta(m^3$（$m^3 \cdot K$）)
Magnetic Fluid	1.3	4200	0.6701	9.0×10^{-4}

0.2 m, and pressure value of 0.2 MPa in the sealed shaft section as designed. The material of the simulated permanent magnet is N38-H in NdFeB; the main shaft is made of #45 steel; and the housing is made of a non-magnetic Al alloy (model YL102).

The setting of the magnetofluid material is added in a user-defined manner. The relevant parameters of the magnetofluid are shown in Table 2.

Other setting conditions of the simulation are as follows: an ambient temperature of 25 °C and relative permeability of MURX1.0. Because the magnetofluid sealing device is distributed along the circumference of the main shaft, the magnetization direction of the permanent magnet only needs to be changed in the YOZ plane and overlapped with the axial direction (X direction) of the main shaft. The magnitude of the coercive force of the permanent magnet block is 0.975 A/m in the following distribution as shown in Fig. 7.

Some areas need to be densified by user-defined meshing for the difference in dimensions of various parts of the sealing device. The maximum grid size of the magnetofluid part is 0.02 mm, the maximum grid size of the permanent magnet is 0.5 mm, and the maximum grid size of the main shaft and the housing is 1 mm.

B. MAGNETIC RESULTS AND ANALYSIS

The magnetofluid sealing device is symmetrically distributed along the main axis, with the XOY plane and the YOZ plane chosen for the analysis of the magnetic field simulation results. According to the magnetofluid sealing device diagram, however, the middle sealing clearance of the permanent magnet in the direction of X is far greater than the sealing clearance at both ends. Therefore, the representative surface YOZ plane is translated by 20 mm along the X direction to explore the magnetic field distribution of parts with smaller clearance. The cloud charts and vector diagrams for the magnetic field analysis are shown in Fig. 8.

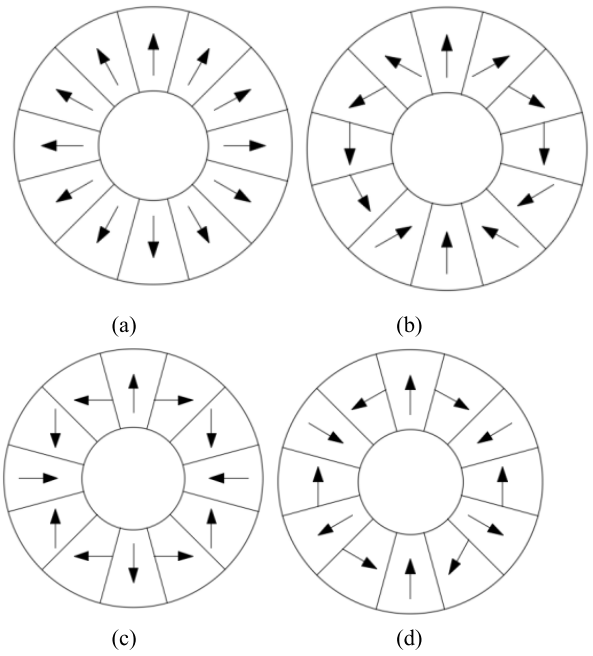

FIGURE 7. Four Halbach magnetic matrix magnetization directions: (a) is type I, (b) is type II, (c) is type III, (d) is type IV.

According to the simulation results and the observations of the cloud charts of type I, II, III, and IV on the XOY plane, there is a magnetic-free area at the center of the type-I and type-III main shafts; the type-I structured magnetic-free area is mainly distributed along the Y-axis direction, and the type-III structured magnetic-free area is distributed along the X-axis direction. According to the observations of the vector diagrams of type I, II, III, and IV on the XOY plane, there are four distinct circular magnetic loops of type I, II, III, and IV structures at the edges of the magnetic poles. According to the observations of the cloud charts of type I, II, III, and IV on the YOZ plane, all of the four Halbach magnetic arrays have mid-enhanced magnetic characteristics, which are consistent with Halbach magnetic array research. However, the side-reinforcement of the type-I structure has a small radial depth, while the type-III structure has the largest radial depth of approximately 20 mm, followed by the type-IV structure with a radial depth of approximately 15 mm and the type-II structure with a radial depth of approximately 10 mm. According to the observations of the vector diagrams of type I, II, III, and IV on the YOZ plane, the magnetic force of the type-I structure shows direct radial radiation in a circular shape; there are

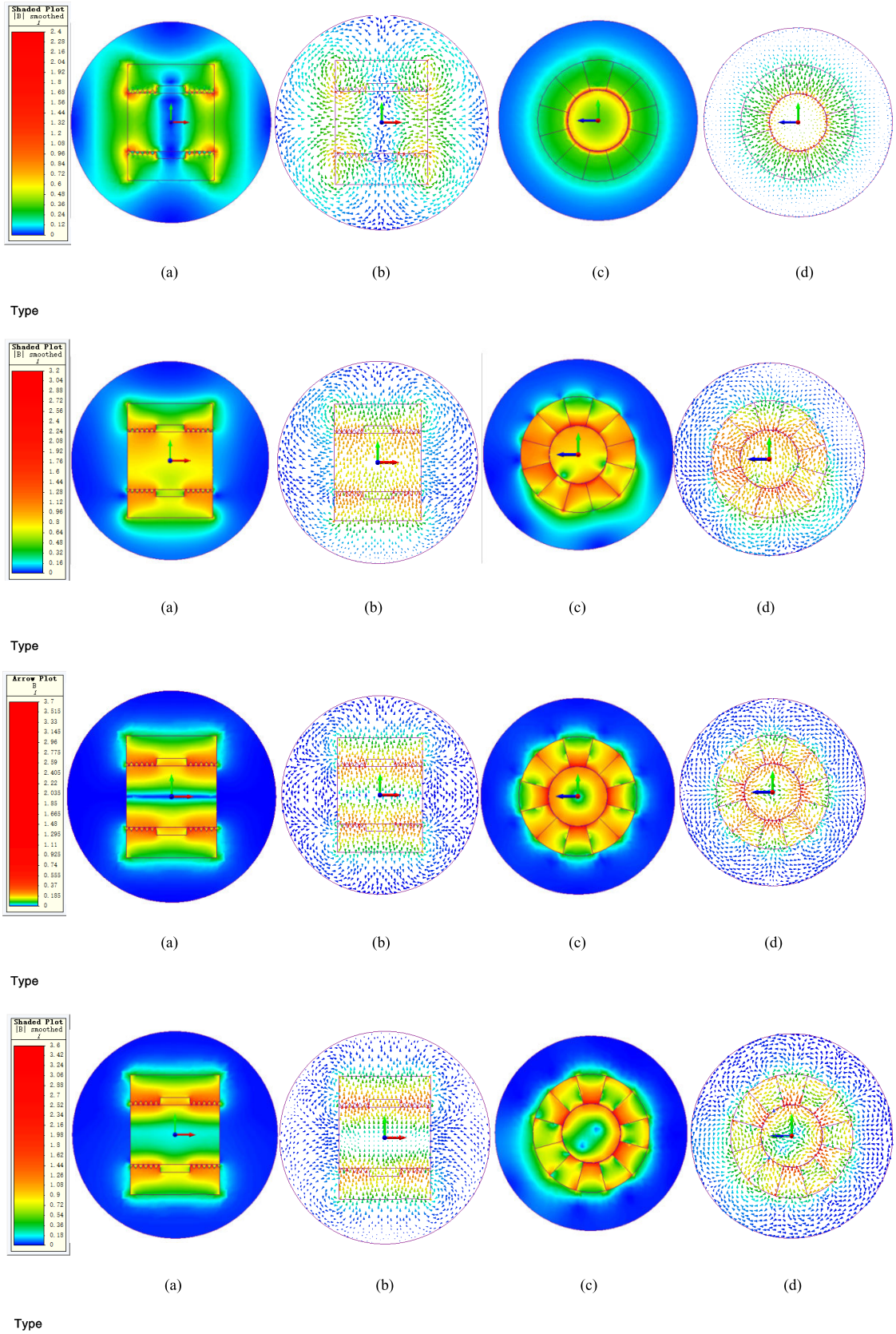

FIGURE 8. Simulation results: (a) is the cloud chart of the XOY plane, (b) is the vector diagram of the XOY plane, (c) is the cloud chart of the translated YOZ plane, (d) is the vector diagram of the translated YOZ plane).

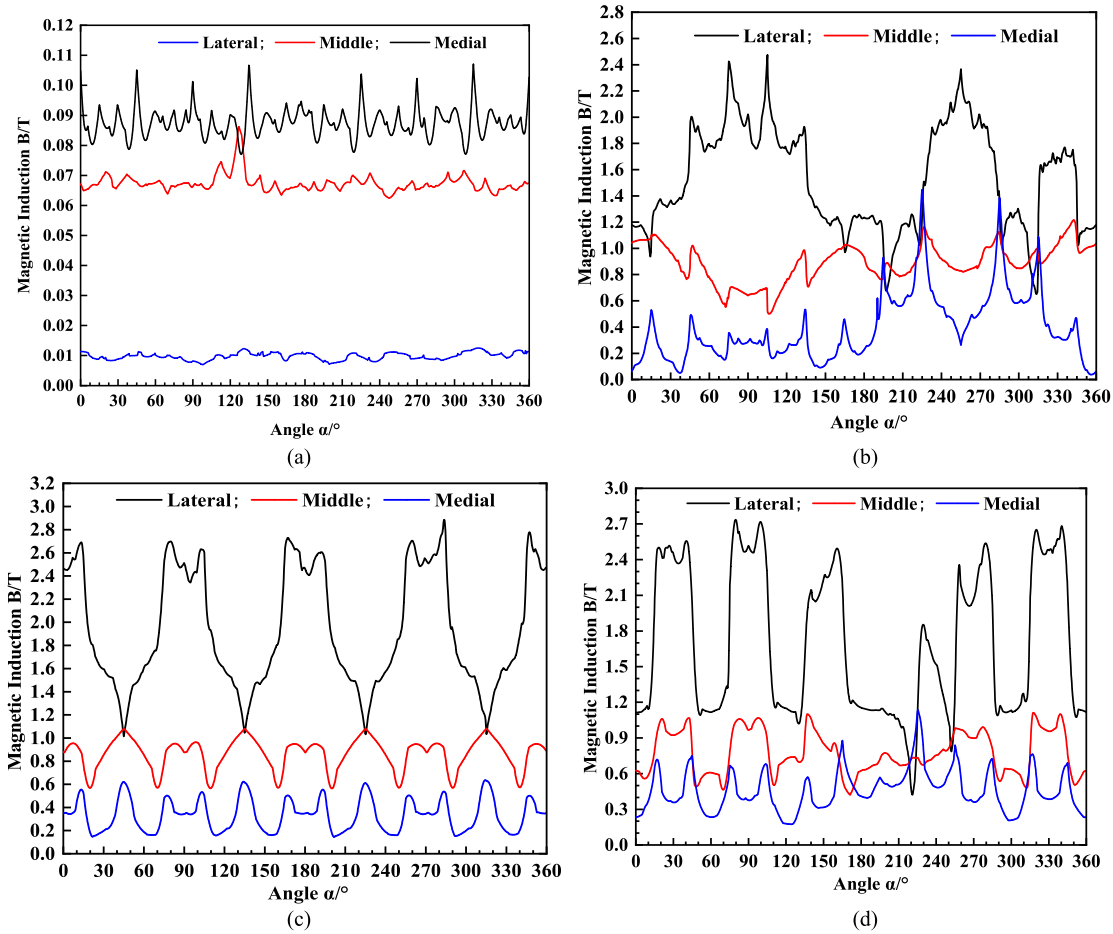

FIGURE 9. Magnetic field values of four Halbach magnetic arrays at different radial depths: (a) represents type I, (b) represents type II, (c) represents type III, (d) represents type IV.

four, four, and six magnetic loops of magnetic force for the type-II, type-III, and type-IV structures on the main shaft.

The main reason for the above phenomenon is as follows: a radial magnetic-free area forms in the middle of the type-I structure in the cloud chart on the XOY plane, as magnetization of the type-I structure is radial along the main shaft axis, thus preventing the formation of a magnetic return path for the magnetofluid sealing structure in the structure, so a magnetic return path can only form at the boundary (air dome). The phenomenon corresponds to the XOY plane vector diagram of the type-I structure in Fig. 8, with the circuits offsetting on the mid-y axis. Therefore, the area in the radial direction is magnetic-free. For the magnetic-free area of the type-III structure formed in the direction of the main shaft, according to the type-III structure in the YOZ vector diagram as shown in Fig. 8, the four magnetic loops of the main shaft area of the structure are symmetrically distributed along the axis, thus leading to superposition and emergence of an axial magnetic-free area on the main shaft axis. In the XOY plane vector diagram, according to the magnetization direction, all of the four Halbach magnetic array methods have a unilaterally reinforced structure, so the magnetic induction intensity near the interior of the main shaft is higher and the outer magnetic induction intensity value is lower, thus resulting in the formation of magnetic loops.

In the YOZ planar cloud and vector graph, according to the magnetizing directions, the magnetizing direction of the type-I structure is outward along the radial direction of the main shaft. Therefore, a loop can only be formed at the poles and borders, but not inside the magnetofluid sealing clearances. For type II, III, and IV, there exists superposition of the units of the magnetic field. In structure II and III, three magnetic blocks form one unit and the directions of the two magnetic blocks are nearly vertical. Therefore, there are six magnetic loops. However, the increasing number of magnetic loops will lead to interactions between different magnetic paths, so there will be more magnetic energy loss. The largest value for the type-IV magnetic strength was smaller than that for the type-III structure. As for the radial depth of all structures, the larger magnetic strengths of the internal side of the magnetofluid sealing structure were associated with a bigger the gradient range of the main shaft axis. Therefore, the radial strength of all structures changes accordingly with the maximum magnetic strength, that is, type III > type IV > type II > type I.

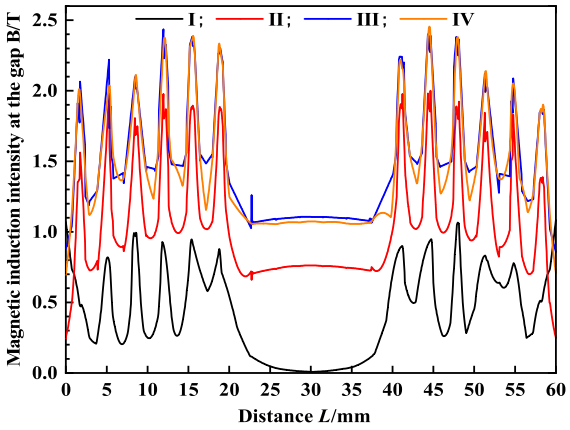

FIGURE 10. Magnetic field value of the seal gap.

TABLE 3. Theoretical pressure capacity calculation table.

Type	I	II	III	IV
Minimum magnetic induction at the gap (B_{max}/T)	1.0572	1.9483	2.4352	2.3641
Maximum magnetic induction at the gap (B_{min}/T)	0.2873	0.9034	1.2746	1.1662
Theoretical pressure resistance (MPa)	0.346455	0.470205	0.52227	0.539055

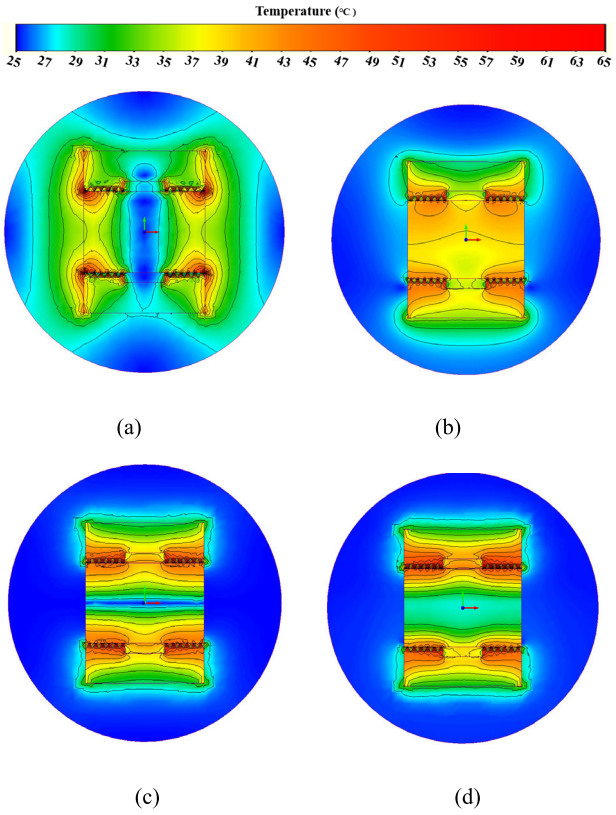

FIGURE 11. Temperature field cloud diagram of the magnetic fluid seal: (a) represents type I, (b) represents type II, (c) represents type III, (d) represents type IV.

To determine the specific effect of the magnetic field strengthened by the Halbach magnetic array and magnetic strength of sealing clearances, in the simulation, the software was used to make further calculations on the magnetic fields. The calculation results are shown in Figs. 9 and 10. Fig. 9 lists the magnetic field values of the four types of magnetic arrays with different radial depths in the YOZ cloud graph. The internal side R = 20.2 mm, the middle part R = 30 mm, and the external side R = 40 mm. Fig. 10 shows the XOY planar cloud graph for the magnetic values of sealing clearances, and the range of linear coordinates is from (−30, 0, 0) to (30, 0, 0).

From the magnetic values of the four types of Halbach magnetic arrays with different radial directions, in the structures I, II, III, and IV, by comparing the magnetic strengths of the part near the magnetofluid (internal side) of all structures, the conclusion can be drawn that the magnetic strength of structure I, which is about 0.09 T, is far smaller than that of the other structures. The values for the middle part and external part are relatively small. The value for the middle part is 0.69 T, and that for the external part is approximately 0.01 T. The magnetic energy utilization rate of this structure is thus relatively low. Besides, the magnetic field of this structure fluctuates fiercely around the whole circle, with basically no stable length. For structures II, III, and IV, the values of internal magnetic strength do not differ greatly, and all are within the range of 2.4 T and 2.8 T. However, structure II is not that stable, which is similar to structure I. The fluctuation is very intense, without a relatively stable length. For the middle and external part of structures III and IV, the changing trend is similar to that of the internal side. In these two structures, there are stable lengths for approximately 30° of the angle of circumference. There are also approximately five pulse times.

The main causes of the aforementioned phenomenon are as follows: all the four types of Halbach magnetic arrays applied in this experiment result in unilateral strengthening. Therefore, as shown in Fig. 9, the magnetic field value of the internal side is the largest, followed by the middle part, and then the external part. Furthermore, in structure I, the magnetizing method of the 12 permanent magnets is outward along the radial direction of the main shaft. This is similar to a single cylinder-shaped permanent magnet. However, in structures II, III, and IV, there are units between which superposition occurs in the sealing clearances to enhance the magnetic energy of the internal side. Therefore, the magnetic strengths of structures II, III, and IV are substantially larger than that of structure I. As indicated in Fig. 8(c), for structures II, III, and IV, there are holes at the center of the main shaft. There are two holes in structure II and IV, and the hole in structure III is concentrated in the main shaft center. Meanwhile, as observed

TABLE 4. Magnetic fluid related parameters.

Type	Base Fluid	Density (kg/m^3)	Viscosity (mPa·s) (25°C)	Saturation Magnetization (KA/m)	Initial Susceptibility (m/H)	Surface Tension (N/cm)	Thermal Conductivity [W/(m·K)]	Specific Heat [kJ/(m3·K)]	Thermal Expansion Coefficient [m^3/(m^3·K)]
MFO3	oil	1.32×10^3	200	450±50	0.8	28×10^{-5}	0.15	1715	9.0×10^{-4}

TABLE 5. Table of instruments required for testing.

Number	Parameters	Type	Instrument	Manufacturer	Range	Precision
1	Magnetic Field Intensity	SG-42	Teslameter	Xi'an Qingcheng Electromechanical Equipment Co., Ltd.	0~2T	±1%
2	Inlet Pressure	Y-61A-Z	Pressure Gauge	Shanghai Automation Instrumentation Co., Ltd.	0~4000KPa	2 Level Precision
3	Outlet Pressure	Y-61A-Z	Pressure Gauge	Shanghai Automation Instrumentation Co., Ltd.	0~4000KPa	2 Level Precision
4	Flow Channel Pressure Difference	YZS-102	Pressure Gauge	Shanghai Automation Instrumentation Co., Ltd.	0~2500KPa	2 Level Precision
5	Torque	TL-303	Torque Sensor	Beijing AVIC Tailong Technology Co., Ltd.	0±100N.m	±1%
6	Speed	SF120E	Digital Governor	Dongguan Haoran Electromechanical Equipment Co., Ltd.	0~3200r/min	±0.5r/min
7	\	YE2-160	Three-phase Asynchronous Motor	Botou Zhengkang Environmental Protection Equipment Co., Ltd.	\	\
8	Temperature	KZW-JPT -A	Temperature Sensor	Beijing Kunlun Zhongda Sensor Technology Co., Ltd.	-200°C~450°C	±0.2%

from Fig. 8(c), in structure II, the holes are located in the Y side, and in structure IV, the holes are central and symmetrical around the point of origin. According to the fluctuations shown in Fig. 9, the existence of holes has a direct impact on the fluctuations of the internal and external side of magnetofluids. The number of holes is directly proportional to the fluctuation condition. The symmetrical holes will affect each other, which will, to some extent, weaken the fluctuations caused by the holes. In structures III and IV, there are stable lengths in the range of approximately 30°. This phenomenon occurs because there are a total of 12 permanent magnets in the entire magnetofluid sealing device, and when evenly distributed on the circle, each magnetic block takes up the area of about 30°, while the solid structure of each magnetic block does not move.

As shown in Fig. 10, which presents the magnetic field values of sealing clearances, in structure I, II, III, and IV, the general trends and fluctuations of the four types of structure are almost the same. However, the value for structure I is the smallest, with the largest value at the polar teeth of approximately 1.0 T; structure II follows next, where at the polar teeth the largest value is about 2.42 T. The values for structures III and IV are the largest, while the largest value at the polar teeth is about 2.75 T. However, taking (9) and the boundary conditions into consideration, the rotational speed of the hydroturbine of different models is 300 r/min, so in (9), the centrifugal force is the same. When primarily selecting a Halbach magnetofluid sealing structure, the subtractor is the same, so the optimized structure can be judged by the minuends. Therefore, by simplifying (8):

$$p(B) - p(A) = \frac{1}{\mu_0}\overline{M}\,(B_{\max} - B_{\min}) \tag{26}$$

From (26), to obtain a relatively larger sealing pressure-withstanding value, the maximum magnetic strength difference of the clearance should be specified. On the basis of Fig. 10, the maximum sealing pressure-withstanding values of different structures are further calculated. The calculation results are indicated in Fig. 3. (In theoretical calculations, the MFO3 magnetofluid is chosen, with a saturated magnetic strength of 450 KA/m).

From the calculation results, in structure I, II, III, and IV, the theoretical pressure-withstanding value results are ranked as type IV > type III > type II > type I, with respective values of 0.539055 MPa, 0.52227 MPa, 0.470205 MPa, and 0.346455 MPa.

(a)

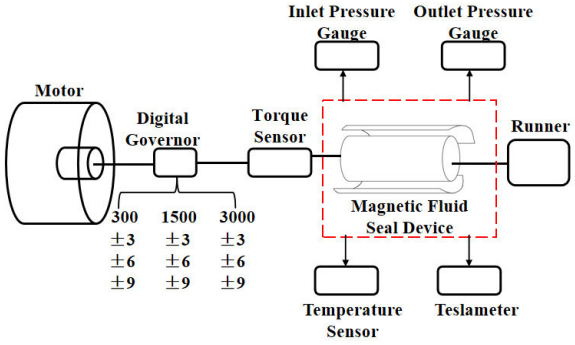

(b)

FIGURE 12. Magnetic fluid spindle seal test bench: (a) photograph of real objects, (b) diagram of the experimental principle.

C. SIMULATION RESULTS AND ANALYSIS FOR THE TEMPERATURE FIELD

The analysis results for the temperature field of the main shaft magnetofluid sealing device of the hydroturbine are shown in Fig. 11. structure. From the simulation results, the highest temperature of the temperature field of structure I is 60 °C. The areas of the highest temperature are mainly located in the polar teeth or at the junction of the magnetic pole and shell. The temperature at the middle of the permanent magnet and the radial direction of the middle of the main shaft is almost the same as the set environmental temperature, which is 25 °C. The maximum value of structure II, which is 65 °C, is the largest among all of the four structures. The area with the highest temperature is located in the polar teeth. The temperature decreases along the radial direction from the polar teeth. For structure III and IV, the highest temperature of the temperature field is similar to that in structure I, which is at 60 °C. Additionally, the area with the highest temperature is located at the polar teeth, and the temperature decreases along the radial direction from the polar teeth. The comparison between structures III and IV shows that the middle part along the axial direction of structure III is room temperature.

The reasons for such a phenomenon are as follows: during the simulation calculation process, the magnetofluid in the sealing clearances has the nature of ordinary fluid and can cool down the heat at the polar teeth, thus leading to the result

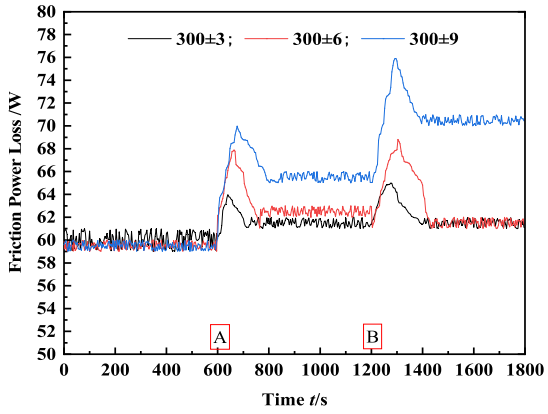

(a)

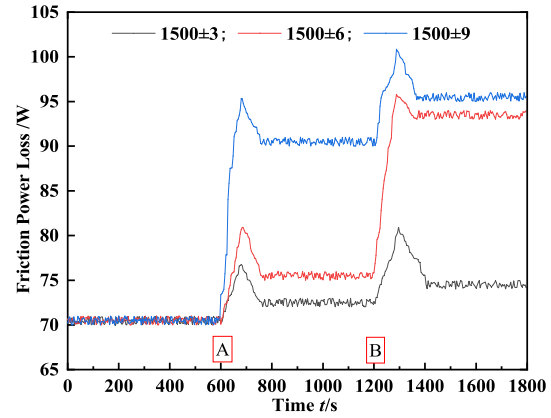

(b)

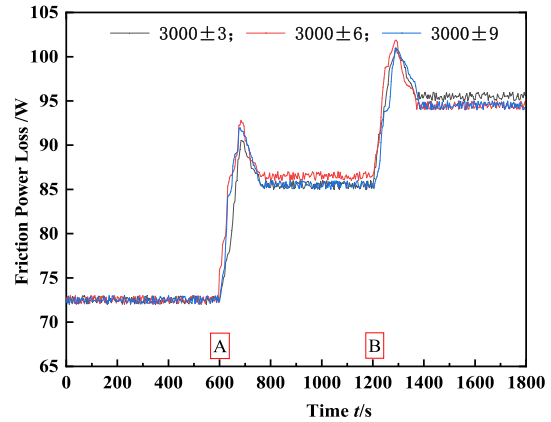

(c)

FIGURE 13. Friction power consumption diagram of the Halbach magnetic fluid seal device under random operating conditions at different speeds: (a) 300 r/min, (b) 1500 r/min, (c) 3000 r/min.

that the middle part of the sealing clearances is obviously small. However, the magnetic strength is the strongest at the polar teeth area of the magnetofluid sealing device, and from (24) and (25), the friction power consumption is the most obvious at the polar teeth. The external indicator is that the temperature rises the most at the highest value. On the basis

of the YOZ planar magnetic strength from Fig. 9, there are magnetic fluctuations on the circle in structures I and II, so the magnetic forces asserted on the magnetofluids of each part of the circle are not even. As a result, the magnetofluid, which rotates under the force of the main shaft, will have a relatively strong asymmetric curl (as indicated in (18) and (19)). The friction force is relatively strong, and the external temperature rise is significant. For structure I, the maximum magnetic strength is relatively small, so the magnetofluid friction caused by fluctuations is not significant, nor is the temperature rise. For structure II, the maximum magnetic strength is relatively large, so the friction caused by friction is obvious, and so is the temperature rise. Besides, the maximum magnetic strengths of structures II, III and IV are close, and the highest temperature caused by fluctuations reached the largest value in structure II.

By having an overall look at the magnetic force, the magnetic fluctuations, and the asymmetry, structure III was selected as the optimal structure for the experiment.

IV. ANALYSIS OF THE EXPERIMENTAL RESULTS

According to the numerical analysis results, under the rotational speed of 300 r/min, the four types of hydroturbine main shaft magnetofluid sealing structures with different Halbach magnetic arrays were filtered and structure III was selected as the experimental model.

The scale between the model and the actual size is 1:5. In the experiment, the rotational speeds of the motor were 300, 1500, and 3000 r/min. After the motor was running stably, we changed the rotational speed in order to perform tests under alternating work conditions of ± 3, ± 6, and ± 9. The magnetofluid main shaft sealing test stand is shown in Fig. 12. The parameters related to the magnetofluid and equipment used in the experiment are shown in Tables 4 and 5.

A. RESULTS AND ANALYSIS FOR THE FRICTION POWER CONSUMPTION

The friction power consumption of the hydroturbine main shaft magnetofluid sealing device with Halbach structure III was measured by the rotational speed meter and the torque sensor under random work conditions of 300, 1500, and 3000 r/min, and the results are shown in Fig. 13. Point A represents the time point when the speed increases, and point B represents the time point when the speed decreases.

According to the results of the friction power consumption experiment, as the rotational speed increases, the friction power consumption of the Halbach magnetofluid sealing device increases gradually. When the rotational speed is higher than 1500 r/min, the friction power consumption increases slowly. Meanwhile, by comparing the friction power consumption under different rotational speeds and random work conditions, it was observed that when the rotational speed is low, the friction power consumption increases as the amplitude of random conditions increases. However, when the rotational speed resumes, the friction power consumption remains almost the same. As the rotational speed increases to medium or high, the friction power consumption significantly increases as the amplitude of the random work conditions increases, and when the rotational speed resumes, the friction power consumption is still considerably larger than the initial value.

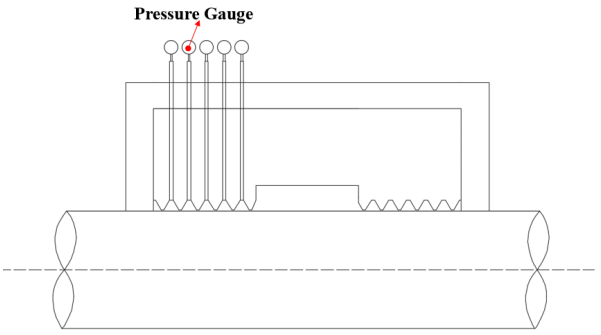

FIGURE 14. Pressure gauge layout.

The reasons for such a phenomenon are as follows: from (17) and (18), as the rotational speed increases, the asymmetric curl of the Halbach magnetofluid sealing device continuously increases. Considering (24) and (25), when the rotational speed increases, the friction power consumption increases accordingly. When the hydroturbine main shaft is operating under a low rotational speed, the hydroturbine rotational speed is changing randomly within a small range, which will, to some extent, increase the friction power consumption of the magnetofluid sealing device. When the rotational speed resumes, because the magnetofluid has a certain thermal conductivity, it can recover by itself, and the friction power consumption will remain almost stable. When the hydroturbine main shaft is operating under medium or high rotational speeds, the ability of the magnetofluid to recover itself is destroyed, so the friction power consumption increases significantly, and the friction power consumption of the device is far larger than the initial value.

B. RESULTS AND ANALYSIS FOR THE SEALING EXPERIMENTS

The pressure-withstanding values of the magnetofluid sealing under alternating work conditions with rotational speeds of 300, 1500, and 3000 r/min were measured by a pressure meter, and the results are shown in Fig. 15 (the arrangement of pressure meters is shown in Fig. 14, and from the left to right, the pressure meters are numbered as 1–5.).

From the experiment results, it can be seen that as the rotational speed increases, the pressure-withstanding values of the hydroturbine main shaft magnetofluid sealing device with a Halbach structure III magnetic array under random work conditions decreases. The smallest rotational speed has a value of approximately 0.45 MPa. When the rotational speed increases to over 1500 r/min, the sealing pressure-withstanding value reaches to nearly 0. When the rotational speed increases to a high speed, the sealing

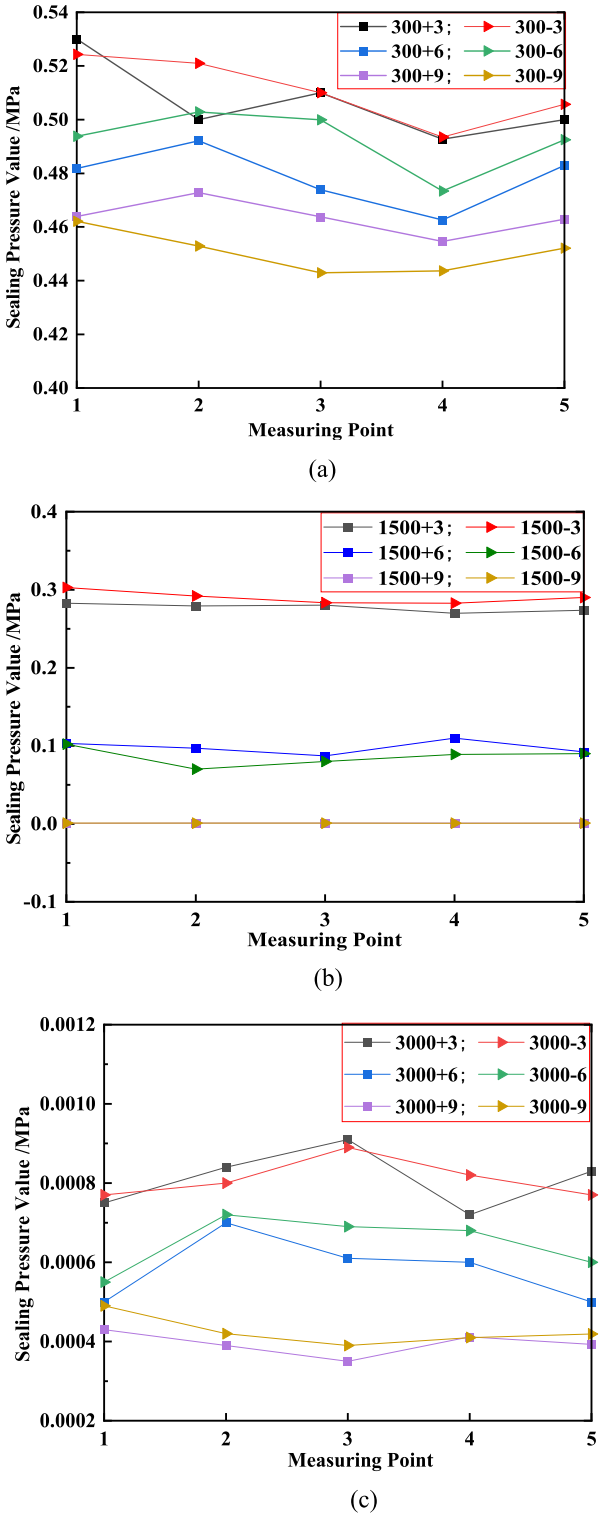

FIGURE 15. Magnetic fluid seal pressure diagram: (a) 300 r/min, (b) 1500 r/min, (c) 3000 r/min.

pressure-withstanding value is almost 0. In the meantime, by observing the alternating work conditions under each rotational speed, it was found that the sealing pressure-withstanding value decreases as the amplitude of the alternating work conditions increases, but this has nothing to do with the rotational speed, i.e., this occurs no matter the increases or decreases in the speed when the amplitude of the alternating work conditions changes. When the hydroturbine main shaft is running at a medium or high speed, the alternating work condition can only be changed within a small range. When the amplitude of the alternating work conditions exceeds a certain value, the magnetofluid sealing is damaged and becomes invalid, thus the sealing pressure-withstanding value is nearly 0.

The reasons for such a phenomenon are as follows: from the magnetofluid sealing in (8), it was found that the pressure-withstanding capacity of the magnetofluid sealing is directly proportional to the magnetic strength difference at the clearances and the magnetization intensity, and inversely proportional to the rotational speeds of the main shaft. Therefore, as the rotational speed increases, the pressure-withstanding value of the magnetofluid sealing device continuously decreases. Considering (18) as well as (24) and (25), the friction power consumption of the magnetofluid sealing device is directly proportional to the rotational speed. Friction power consumption usually is accompanied by heat. Considering (22), the magnetizing intensity of the magnetofluid is directly connected with the temperature at which the magnetofluid is in. The temperature increases, while the magnetizing intensity decreases. As shown in Fig. 13, the results indicate that when the rotational speed is medium or high, the friction power consumption of magnetofluid sealing increases significantly, thus generating substantial heat; this considerably reduces the magnetizing intensity of the magnetofluid. Consequently, the sealing becomes invalid, and the sealing pressure-withstanding value reaches nearly 0.

V. CONCLUSION

On the basis of existing magnetofluid sealing theories, the equations for the pressure-withstanding value of the hydroturbine main shaft magnetofluid sealing device and the friction power consumption caused by asymmetric curls were deduced. It has been determined that the external magnetic field and the rotational speed have real impacts on the magnetofluid and the sealing device. The electromagnetic field and temperature field of ANSYS was leveraged to perform numeric simulation calculations on the magnetofluid sealing device with Halbach magnetic arrays to select the optimal magnetic energy structure with the highest efficiency. Then, the friction power consumption and sealing pressure-withstanding value of the Halbach magnetofluid sealing device under alternating work conditions and different rotational speeds were analyzed based on the experiment. According to the numeric simulation and experimental results, the following conclusions were drawn:

1) For a hydroturbine main shaft magnetofluid sealing device, the instability of the external magnetic field and the asymmetry against the main shaft will intensify the asymmetric curl of the magnetofluid, thus leading to the result that the friction power consumption increases greatly. The temperature increases greatly too. Besides, the instability of

the external magnetic field and the asymmetry against the main shaft will also impact the stability of the magnetofluid sealing system.

2) For a hydroturbine main shaft magnetofluid sealing device, the external magnetic field will lead to asymmetric curl of the magnetofluid, which causes friction power consumption and large amounts of heat are generated in the sealing clearances. Correspondingly, the magnetizing intensity of the magnetofluid is weakened, so is the pressure-withstanding capacity of the magnetofluid sealing.

3) For a hydroturbine main shaft magnetofluid sealing device, as the rotational speed of the main shaft increases, the centrifugal forces of the magnetofluid will be increased, thus the sealing pressure-withstanding value of the magnetofluid sealing will be lowered. In addition, the increase in the rotational speed will lead to a relatively large friction power consumption of the magnetofluid, with the generation of a considerable amount of heat and a lowered magnetizing intensity, which will further reduce the pressure-withstanding value of the magnetofluid sealing device.

REFERENCES

[1] International Hydropower Association (IHA), *Hydropower Status Report Industry Trends and Reflections*. Beijing, China: China Water Resources and Hydropower Press, 2018, p. 12.

[2] W. Yao, "Hydropower development in the context of global energy interconnection," *Water Resour. Hydropower Lett.*, vol. 39, no. 3, pp. 4–5 and 9, 2018.

[3] B. J. Yang, Y. F. Ji, and C. B. Wu, "Leakage analysis and treatment of main shaft seal of Unit 2 ~# of Tai'an pumped storage power station," *Water Resour. Hydropower Eng.*, vol. 48, no. S1, pp. 107–109, 2017.

[4] X. G. He, "Optimization and improvement of the seal structure of the main shaft of the turbine of the Mi Mipo mixed-flow unit," *Water Resour. Hydropower Eng.*, vol. 45, no. 12, pp. 86–90, 2014.

[5] J. P. Zhai and H. H. Liao, "Failure analysis and treatment of water leakage in the turbine shaft seal," *Lubrication Sealing*, vol. 36, no. 12, pp. 104–106 and 116, 2011.

[6] K. P. Chen, "Analysis and countermeasures for the breakage of the connecting bolt between the runner and the main shaft of the bulb tubular unit," *China Rural Water Hydropower*, vol. 10, no. 10, pp. 134–137, 2016.

[7] Y. F. Wei, "Installation and operation of turbine spindle seal of Iran's Kalun III power station," *Large Motor Technol.*, vol. 2, no. 10, pp. 48–49, 2009.

[8] D. Momčilović, Z. Odanović, R. Mitrović, I. Atanasovska, and T. Vuherer, "Failure analysis of hydraulic turbine shaft," *Eng. Failure Anal.*, vol. 20, pp. 54–66, Mar. 2012.

[9] R. E. Chupp, F. Ghasripoor, N. A. Turnquist, M. Demiroglu, and M. F. Aksit, "Advanced seals for industrial turbine applications: Dynamic seal development," *J. Propuls. Power*, vol. 18, no. 6, pp. 1260–1266, Nov. 2002.

[10] H. K. Müller, *Fluid Sealing Technology: Principles and Applications*. Evanston, IL, USA: Routledge, 2019.

[11] R. E. Rosensweig, *Ferrohydrodynamics*. New York, NY, USA: Cambridge Univ. Press, 1985.

[12] A. Berkowitz, J. Lahut, and C. VanBuren, "Properties of magnetic fluid particles," *IEEE Trans. Magn.*, vol. MAG-16, no. 2, pp. 184–190, Mar. 1980.

[13] S. Kamiyama, "A magnetic fluid actuator," *J. Robot. Soc. Jpn.*, vol. 2, no. 4, pp. 325–329, 1984.

[14] J.-C. Bacri, A. O. Cebers, and R. Perzynski, "Behavior of a magnetic fluid microdrop in a rotating magnetic field," *Phys. Rev. Lett.*, vol. 72, no. 17, pp. 2705–2708, Apr. 1994.

[15] Y. S. Kim and Y. H. Kim, "Application of ferro-cobalt magnetic fluid for oil sealing," *J. Magn. Magn. Mater.*, vol. 267, no. 1, pp. 105–110, Nov. 2003.

[16] T. Hayat, S. A. Shehzad, and A. Alsaedi, "Soret and Dufour effects on magnetohydrodynamic (MHD) flow of Casson fluid," *Appl. Math. Mech.*, vol. 33, no. 10, pp. 1301–1312, Aug. 2012.

[17] T. Hayat, M. Qasim, and Z. Abbas, "Radiation and mass transfer effects on the magnetohydrodynamic unsteady flow induced by a stretching sheet," *Zeitschrift Naturforschung A*, vol. 65, no. 3, pp. 231–239, Mar. 2010.

[18] D. Hu, Y. Wang, and Z. Pan, "Stability and magneto-rheological properties of magnetic fluids containing Fe_3O_4 nano-particles with different morphologies," *J. Chin. Ceram. Soc.*, vol. 40, no. 4, pp. 583–589, 2012.

[19] C. Q. Chi, *The Physics Foundation and Application of Ferrofluid*. Beijing, China: Beijing Univ. of Aeronautics and Astronautics Press, 2011, p. 11.

[20] D. C. Li, *Theory and Application of Magnetic Liquid Sealing*. Beijing, China: Science Press, 2010.

[21] A. V. Radionov, A. D. Podoltsev, and A. A. Radionova, "Express–method for determining the quality of a magnetic fluid for operation in the working gap of a magnetic fluid seal," in *Proc. IOP Conf. Ser., Mater. Sci. Eng.*, Aug. 2017, vol. 233, Art. no. 012038.

[22] J. Liu, "Numerical analysis of secondary flow in the narrow gap of magnetic fluid shaft seal using a spectral finite difference method," *Tribol. Trans.*, vol. 59, no. 2, pp. 309–315, Apr. 2016.

[23] S. M. Lund and K. Halbach, "Iron free permanent magnet systems for charged particle beam optics," Lawrence Livermore Nat. Lab., Livermore, CA, USA, 1995.

[24] K. Halbach, "Use of permanent magnets in accelerator technology: Present and future," in *Proc. MRS*, Feb. 2011, p. 96.

[25] X. Bai, "The well-posedness theory and asymptotic behavior of fractional-order Navier–Stokes equations and the overall well-posedness of a class of large initial value solutions of magnetic fluid equations," *China Acad. Eng. Phys.*, Apr. 2018.

[26] D. F. Bian, *Research on Mathematical Theory of Compressible Fluid Mechanics With Energy Conservation Equation*. Sichuan, China: China Academy of Engineering Physics, 2014.

[27] Z. Hu, Z. Wang, W. Huang, and X. Wang, "Supporting and friction properties of magnetic fluids bearings," *Tribol. Int.*, vol. 130, pp. 334–338, Feb. 2019.

[28] K. N. Dzhumagulova, R. U. Masheyeva, and T. S. Ramazanov, "Effect of magnetic field and friction force on the velocity autocorrelation in two-dimensional Yukawa liquids," *Contrib. Plasma Phys.*, vol. 59, no. 6, Mar. 2019, Art. no. e201800169.

[29] P. Zhang, K. H. Lee, and C. H. Lee, "Fretting friction and wear characteristics of magnetorheological fluid under different magnetic field strengths," *J. Magn. Magn. Mater.*, vol. 421, pp. 13–18, Jan. 2017.

[30] O. N. Labkovich, A. G. Reks, and V. A. Chernobai, "The friction control of magnetic fluid in the Couette flow," *J. Magn. Magn. Mater.*, vol. 431, pp. 91–93, Jun. 2017.

[31] V. M. Polunin, P. A. Ryapolov, A. I. Zhakin, A. M. Ivanov, and E. V. Shel'deshova, "Magnetoviscous effect in case of magnetic fluid oscillations in strong magnetic field," *Magnetohydrodynamics*, vol. 54, no. 4, pp. 353–360, 2018.

[32] F. R. Cunha and Y. D. Sobral, "Characterization of the physical parameters in a process of magnetic separation and pressure-driven flow of a magnetic fluid," *Phys. A, Stat. Mech. Appl.*, vol. 343, pp. 36–64, Nov. 2004.

[33] M. Rasa, "Magnetic properties and magneto-birefringence of magnetic fluids," *Eur. Phys. J. E*, vol. 2, no. 3, pp. 265–275, Jul. 2000.

ZHENGGUI LI was born in Lanzhou, Gansu, China, in 1974. He received the B.S. degree in mechanical engineering and control from the University of Gansu Industry, Gansu, in 1999, and the M.S. degree in hydraulic turbine regulation and the Ph.D. degree in fluid machinery and engineering from the Lanzhou University of Technology, Gansu, in 2006 and 2014, respectively. He is currently a Professor with the School of Energy and Power Engineering, Xihua University. His research interest includes the cross product development of fluid machinery and magnetic technology and the research of magnetic fluid seal and magnetic suspension bearing of hydraulic machinery.

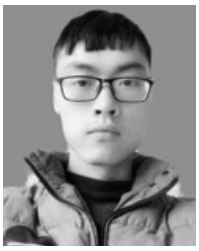

JIE CHENG was born in Dazhou, Sichuan, China, in 1996. He received the B.S. degree in energy and power engineering from Xihua University, Sichuan, in 2019, where he is currently pursuing the M.S. degree in fluid mechanics and engineering. His research interest includes fluid mechanics and engineering.

DEYOU LI was born in Harbin, Heilongjiang, China, in 1986. He received the B.S. degree in thermal energy and power engineering, the M.S. degree in fluid machinery and engineering, and the Ph.D. degree in power machinery and engineering from the Harbin Institute of Technology, Heilongjiang, in 2010, 2012, and 2017, respectively. He is currently an Associate Professor with the School of Energy and Science Engineering, Harbin Institute of Technology. His research interest includes the study of fluid mechanical flow mechanism and flows control strategy.

XIAOHUI DENG was born in Yibin, Sichuan, China, in 1999. She received the B.S. degree in water conservancy and hydropower engineering from Xihua University, Sichuan, in 2017. Her research interest includes hydraulic machinery and engineering.

BING DONG was born in Zhangye, Gansu, China, in 1999. He received the B.S. degree in energy and power engineering from Xihua University, Sichuan, China, in 2017. His research interests include fluid mechanics and finite element analysis.

XIAOBING LIU was born in Langzhong, Sichuan, China, in 1965. He received the B.S. degree in hydromechanics from Sichuan University, Sichuan, in 1985, and the M.S. degree in fluid machinery and engineering and the Ph.D. degree in hydropower engineering from the Huazhong University of Science and Technology, Guangdong, China, in 1992 and 1995, respectively. His research interests include fluid mechanical multiphase flow theory, and numerical and experimental techniques.

BIAO MA was born in Hangzhou, Zhejiang, China, in 1988. He received the B.S. degree in energy and power engineering and the M.S. degree in fluid machinery and engineering from the Lanzhou University of Technology, Lanzhou, China, in 2011. He is the author of eight articles. His research interest includes fluid machinery and engineering.

XINRUI LI was born in Wuwei, Gansu, China, in 1988. He received the B.S. degree in thermal energy and power engineering from Qingdao University, Qingdao, China, in 2012. He is currently pursuing the M.S. degree in energy and power engineering with Xihua University, Sichuan, China, in 2019. His research interest includes fluid machinery.